Analysis of voltammograms of quasi-reversible redox systems: transformation to potential program invariant form

Tamás Pajkossy
Institute of Materials and Environmental Chemistry
Research Centre for Natural Sciences, Hungarian Academy of Sciences
Magyar tudósok körútja 2, Budapest, Hungary, H-1117
e-mail: pajkossy.tamas@ttk.mta.hu

Soma Vesztergom
Department of Physical Chemistry, Eötvös Loránd University,
Pázmány Péter sétány 1/A, Budapest, Hungary, H-1117

Abstract

A simple procedure has recently been suggested (T. Pajkossy, *Electrochem. Comm.* **90** (2018) 69) by which various types of voltammograms, above all cyclic voltammograms, pertaining to partially diffusion controlled charge transfer reactions can be analysed. Using this procedure, from voltammograms taken with varied scan-rates or other-than-triangular waveforms two scan-rate independent, hysteresis-free functions can be calculated. One of them is the diffusion-free polarization curve; the other the semiintegrated form of the reversible voltammograms. Here we show the underlying theory in details, along with numerical simulations to highlight important properties of the transformation. The theory opens a new route for the determination of charge-transfer rate coefficients of quasi-reversible redox systems.

Keywords: diffusion, charge transfer, semiintegration, kinetics, redox system

1. Introduction

Voltammetry is a basic experimental method for studying the kinetics of electrode processes: the current density as a function of time, $j(t)$, is measured, while potential is varied as $E(t)$: voltammograms are the *j* vs *E* plots. Most often – in cyclic voltammetry (CV) measurements – the potential is scanned between two limits usually with a constant absolute value of the scan-rate $v = dE/dt$. Both $j(t)$ and $j(E)$ are complicated functions of v; hence comparison of two CVs measured with different scan-rates is far from being trivial. The comparison is even more complicated if the scan-rate varies in time or when two voltammograms are measured with different, arbitrary waveforms.

In rare, simple cases, however, there exist mathematical transformations by which voltammograms taken at different scan-rates can be transformed to the one-and-the-same $T(E)$ state function – that does not "remember" the actual form of $E(t)$ and has a hysteresis-free, scan-rate independent form. The voltammograms of reversible redox couples, for example, can be transformed to hysteresis-free polarograpic-wave shaped curves using semiintegration: in this case semiintegrated current as function of potential is the scan-rate independent representation of the measured data [1].

In contrast to the case of reversible CVs, the CVs of redox systems of slower kinetics – of the so-called quasi-reversible systems – cannot be transformed to a single $T(E)$ function. However, as it has recently been demonstrated in a short communication [2], by measuring a set of quasi-reversible CVs with different scan-rates, two such state functions can be obtained by a simple procedure. One of them characterizes charge transfer kinetics, the other diffusion. Having derived the relevant equations, the transformation was tested with one set of simulated quasi-reversible CV curves.

The subject of the present communication is the detailed version of that theory, generalized in three respects. (*i*) Both parties of a redox pair are assumed to be present rather than only one; (*ii*) There is no assumption involved with regard to the exponential dependence of the rate coefficients on potential; (*iii*) The theory applies for voltammograms of any $E(t)$ potential programs rather than to CVs only.

The important features of the theory are highlighted through the transformation of five sets of CVs.

2. Theory

Consider a voltammetry measurement of a quasi-reversible redox system [3] with the condition that both the reduced and oxidized forms are present in the bulk of the electrolyte solution. These species take part in an *n*-electron charge transfer reaction with no detectable intermediates, on a planar electrode. The dependence of the rate coefficients on electrode potential – temporarily, until reaching Eq.11 – is not specified; all what is assumed that they lie in a range to make both the anodic and cathodic reactions partially diffusion controlled. We apply the usual assumptions, that is, the redox system is a minority component of the electrolyte; the effects due to electrolyte resistance and convection are disregarded.

Before starting the experiment, at *t*=0, the concentrations of the reactants are uniform in the electrolyte solution and no current flows: $j(t \leq 0) = 0$. Accordingly, the $E(t)$ potential program – of arbitrary waveform – starts at *t*=0 from the redox-potential of the electrolyte solution. We apply an $E(t)$ potential program that crosses the $E = \varepsilon$ level more than once during the experiment, with different local scan-rates: the aim of the derivation presented below is to calculate reaction rate coefficients at given ε potential values.

Different ways for choosing appropriate $E(t)$ controlling waveforms are illustrated by Fig.1. We can, for example, record linear scan voltammograms (LSVs) repetitively at different scan-rates (Fig.1a); we can also record several cyclic voltammograms at varied scan-rates (Fig.1b); or, alternatively, we can even use an arbitrary continuous waveform that crosses ε a number of times, with different local scan-rates (Fig.1c).

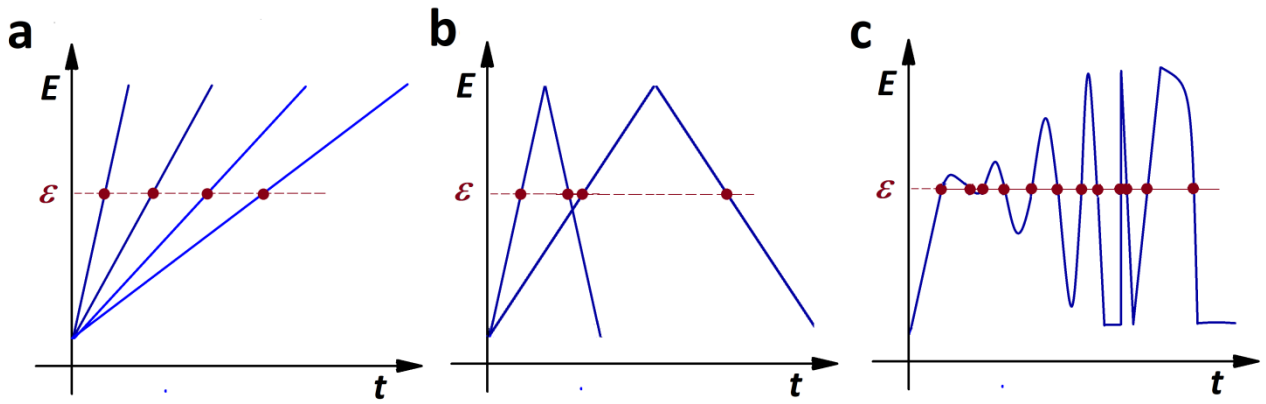

Figure 1. (a). $E(t)$ of typical experiments for which the theory applies. (a) Single scan experiments with varied scan-rates. (b) CVs of varied scan-rates. (c) Voltammograms with arbitrary $E(t)$s, performed with any electric (potentiostatic, galvanostatic, or mixed) control.

The rate of charge transfer is expressed as current desity, *j* in the usual way (Ref. 3, Ch.3) as

$$j = n\mathrm{F}k_{\mathrm{a}}(E)c^{\mathrm{s}}_{\mathrm{red}}(t) - n\mathrm{F}k_{\mathrm{c}}(E)c^{\mathrm{s}}_{\mathrm{ox}}(t) \quad (1)$$

where the superscript s denotes concentrations at the surface and the subscripts a, c, red, and ox refer to anodic and cathodic reactions, and to reduced and oxidized species, respectively; F is Faraday's constant. Note that the k_{a} anodic and the k_{c} cathodic rate coefficients show an explicit dependence only on potential, whereas the $\mathrm{c}^{\mathrm{s}}_{\mathrm{red}}$ and $\mathrm{c}^{\mathrm{s}}_{\mathrm{ox}}$ near-surface concentrations depend explicitly solely on time. The time dependence of the near-surface concentrations is due to the diffusional hindrance of the motion of the redox species. With no hindrance, i.e. at infinite transport rate, the current is denoted by $j_{\mathrm{inf}}(E)$; then, Eq.1 is simplified to

$$j_{\mathrm{inf}}(E) = n\mathrm{F}k_{\mathrm{a}}(E)c_{\mathrm{red}} - n\mathrm{F}k_{\mathrm{c}}(E)c_{\mathrm{ox}} \quad (2)$$

where the concentrations (without suffixes) are bulk ones. When diffusion limitation is present, the near-surface and and bulk concentrations are related to each other through the species flux (here expressed as current density) by the following equations:

$$\mathrm{c}^{\mathrm{s}}_{\mathrm{red}}(\mathrm{t}) = \mathrm{c}_{\mathrm{red}} - \frac{1}{n\mathrm{F}\sqrt{D_{\mathrm{red}}}} \cdot \frac{1}{\sqrt{\pi}} \int_0^t \frac{j(u)}{\sqrt{t-u}}\, du \quad (3a)$$

and

$$c^{\mathrm{s}}_{\mathrm{ox}}(t) = c_{\mathrm{ox}} + \frac{1}{n\mathrm{F}\sqrt{D_{\mathrm{ox}}}} \cdot \frac{1}{\sqrt{\pi}} \int_0^t \frac{j(u)}{\sqrt{t-u}}\, \mathrm{d}u \quad (3b)$$

where D_{red} and D_{ox} are the diffusion coefficients of the two species, and *u* is the convolution auxiliary variable. Eqs 3a and 3b have first been derived by Matsuda and Ayabe in 1955 [4]; similar equations – also in Laplace transformed forms – have been published many times since then; see also Sect. 6.2.1. of Ref. 3. Note that these equations are consequences of the equations of diffusion towards a plane and have no connection whatsoever to the nature of the charge transfer reaction. For other than planar electrode geometries, the convolution terms of Eqs 3a and 3b are to be modified according to the diffusion geometry; this is beyond the scope of the present paper.

In what follows, for the convolution terms of Eqs 3a and 3b we use the name „semiintegrated current" introduced by Oldham [1]; for a detailed analysis see his recent textbook [5]. Semiintegrated current, $M(t)$, is defined as:

$$M(t) = \frac{1}{\sqrt{\pi}} \int_0^t \frac{j(u)}{\sqrt{t-u}} \mathrm{d}u \tag{4}$$

With the combination of Eqs. 1 to 4, we obtain for time τ, when $E = \varepsilon$,

$$j(\tau) = [n\mathrm{F}k_\mathrm{a}(\varepsilon)c_\mathrm{red} - n\mathrm{F}k_\mathrm{c}(\varepsilon)c_\mathrm{ox}] - \left[\frac{k_\mathrm{a}(\varepsilon)}{\sqrt{D_\mathrm{red}}} + \frac{k_\mathrm{c}(\varepsilon)}{\sqrt{D_\mathrm{ox}}}\right] \cdot M(\tau) \tag{5}$$

Combining this equation with Eq.2, and introducing the denotion

$$H(\varepsilon) = k_\mathrm{a}(\varepsilon)/\sqrt{D_\mathrm{red}} + k_\mathrm{c}(\varepsilon)/\sqrt{D_\mathrm{ox}} \tag{6}$$

we arrive at two shorter forms:

$$j(\tau) = j_\mathrm{inf}(\varepsilon) - H(\varepsilon) \cdot M(\tau) \tag{7a}$$

and

$$M(\tau) = (j_\mathrm{inf}(\varepsilon) - j(\tau))/H(\varepsilon) \tag{7b}$$

This latter equation allows us to introduce the *M*-function of reversible voltammograms, $M_\mathrm{rev}(E)$. Consider the $|j(\tau)| \ll |j_\mathrm{inf}(\varepsilon)|$ condition implying a completely diffusion controlled charge transfer; that is, for this case $M(\tau) = M_\mathrm{rev}(\varepsilon)$, hence

$$M_\mathrm{rev}(\varepsilon) = j_\mathrm{inf}(\varepsilon)/H(\varepsilon) \tag{8}$$

Note the proportionality – with a positive proportionality factor – of $j_\mathrm{inf}(\varepsilon)$ and $M_\mathrm{rev}(\varepsilon)$: its consequences are discussed at Point 2 of Discussion.

Finally, with the combination of Eqs. 5 to 8 we arrive at

$$j(\tau) = j_\mathrm{inf}(\varepsilon) - \frac{j_\mathrm{inf}(\varepsilon)}{M_\mathrm{rev}(\varepsilon)} \cdot M(\tau) \tag{9}$$

The course of the j vs M function along with its characteristic values is shown in Fig.2. Eq. 9 represents the basis of extrapolation to infinite rates of diffusion: on a series of voltammograms recorded with varied scan-rates there are a number of ε-crossings $j(\varepsilon)$ points for which $j(M)$ point pairs can be plotted. These points lie on a straight line intersecting the ordinate and the abscissa at j_inf and M_rev, respectively. With increasing scan-rate the points move towards the ordinate.

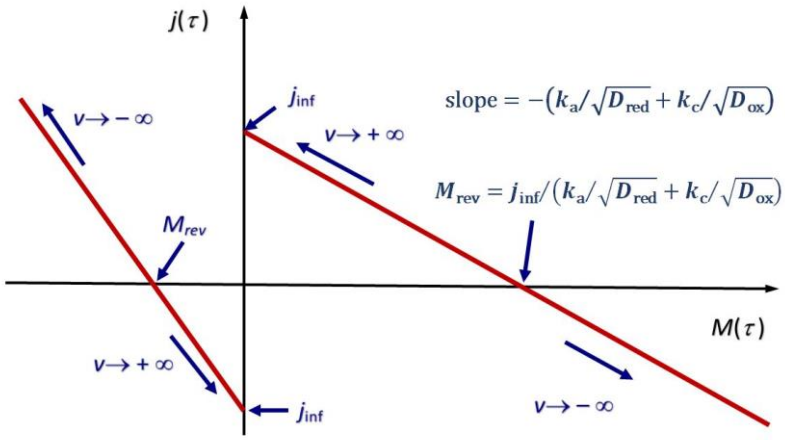

Figure 2. Graphical representation of the quantities of Eqs. 7 and 8. The two lines represent the two cases for which $j_{\text{inf}}(\varepsilon)$ is positive or negative.

Repeating this procedure for all ε s, we get j_{inf} and M_{rev} as a function of potential. Since they depend on potential only, they do not depend on the actual shape of the potential program, by which the *j*s have been measured. In the same vein, since they are single valued functions, they do not exhibit any hystereses.

Eq. 9 is the main result of the theory. This equation is valid irrespectively on the actual form of the dependencies of the rate coefficients on potential. However, if we consider the usual exponential dependences, then we can proceed to get more explicit forms of $j_{\text{inf}}(E)$ and $M_{\text{rev}}(E)$. First, with the introduction of

$$K(E) = [k_{\text{c}}(E)/k_{\text{a}}(E)] \cdot \sqrt{D_{\text{red}}/D_{\text{ox}}} \tag{10}$$

Eq. 8 takes the following form:

$$M_{\text{rev}}(E) = \frac{n\text{F}(k_{\text{a}}c_{\text{red}} - k_{\text{c}}c_{\text{ox}})}{k_{\text{a}}/\sqrt{D_{\text{red}}} + k_{\text{c}}/\sqrt{D_{\text{ox}}}} = -n\text{F}c_{\text{ox}}\sqrt{D_{\text{ox}}} + \frac{n\text{F}c_{\text{red}}\sqrt{D_{\text{red}}} + n\text{F}c_{\text{ox}}\sqrt{D_{\text{ox}}}}{1 + K(E)} \tag{11}$$

Note that $M_{\text{rev}}(E)$ does not depend on the individual rate coefficients but only on their ratio; ie., $M_{\text{rev}}(E)$ is indeed an attribute of diffusion only. As a next step we assume that the *k* rate coefficients exhibit exponential potential dependences as

$$k_{\text{a}}(E) = k_0 \text{exp}\left(\frac{\alpha_{\text{a}}\text{F}(E - E_0)}{\text{R}T}\right) \tag{12a}$$

and

$$k_c(E) = k_0 \exp\left(\frac{-\alpha_c F(E - E_0)}{RT}\right) \tag{12b}$$

where E_0 is the standard redox potential, for the α_a and α_c charge transfer coefficients the $\alpha_a + \alpha_c = n$ equation holds [6], and all other symbols have their usual meaning. In this case, by combining Eqs. 2 and 11, we arrive at the usual form of the Butler-Volmer equation:

$$j_{inf}(E) = nFk_0 c_{red} \exp\left(\frac{\alpha_a F(E - E_0)}{RT}\right) - nFk_0 c_{red} \exp\left(\frac{-\alpha_c F(E - E_0)}{RT}\right) \tag{13}$$

With $\alpha_a + \alpha_c = n$, and Eqs. 12a and 12b, Eq. 10 takes the form:

$$K(E) = \sqrt{\frac{D_{red}}{D_{ox}}} \cdot \exp\left(\frac{-nF(E - E_0)}{RT}\right) \tag{14}$$

By defining the half-wave potential as $E_{1/2} = E_0 + RT/nF \cdot \ln\sqrt{D_{red}/D_{ox}}$ and the cathodic and anodic limit values of $M_{rev}(E)$, respectively, as $M_{lim,c} = -nFc_{ox}\sqrt{D_{ox}}$ and $M_{lim,a} = +nFc_{red}\sqrt{D_{red}}$, Eq. 11 can be rearranged to the form:

$$M_{rev}(E) = M_{lim,c} + \frac{M_{lim,a} - M_{lim,c}}{1 + \exp(-nF(E - E_{1/2})/RT)} \tag{15a}$$

which is just the same as the equations derived by Oldham [7] given in the following forms:

$$M_{rev}(E) = \frac{M_{lim,c}}{2} + \frac{M_{lim,a} - M_{lim,c}}{2} \cdot \tanh\left(\frac{-2nF(E - E_{1/2})}{RT}\right) \tag{15b}$$

and

$$E = E_{1/2} + \frac{RT}{nF} \cdot \ln\left(\frac{M_{rev}(E) - M_{lim,c}}{M_{lim,a} - M_{rev}(E)}\right) \tag{15c}$$

3. Discussion

3.1. Tests of typical cases: numerical simulations

For illustrating the properties of the transformation of Eq.9, five sets of voltammograms (actually CVs) were simulated and made subject to the described transformation. The CVs were generated by a computer program, based on the explicit Euler method for solving the partial differential equation relevant to the transport of the redox species (Appendix B of Ref. 3, [8], taking also into account the quasi-reversible charge transfer and solution resistance. Having calculated the CVs (unless otherwise noted, one complete cycle), the transformation and further calculations have been carried out in the following steps:

a. The semiintegrals were calculated using the algorithm of Ref. 9;

b. The datasets were re-organized to have j vs M data pairs at the same ε potentials (in the case of non-zero R_s, the data pairs should belong to the same $\varepsilon - jR_s$ potentials).

c. According to Eq.9, straight lines were fitted to the $j(\varepsilon)$ vs $M(\varepsilon)$ point pairs by the linear least squares procedure [10]. From the fitted slopes and intercepts M_{rev} and j_{inf} values were calculated for each ε potential. The obtained $j_{\mathrm{inf}}(E)$ and $M_{rev}(E)$ functions were then plotted (Figs.3d,4d,5b,6b,7b). Note that in each simulation, both curves are hysteresis-free; the characteristic values of the curves: typically *M*, j and the $d\log(j)/dE$ slope at $E = E_0$ are exactly the same as can be calculated from the input data. Hysteresis or scatter of the points on the $M_{rev}(E)$ curve is invisibly small in the full potential range; for the $\log(j_{\mathrm{inf}}(E))$ curve scatter appears close to the edges of the potential range; these points are omitted from the plots (the scatter can be traced back to calculation steps with small differences of large numbers).

There were common parameters of the five simulations; these were as follows. Spatial grid size and time resolution: 10^{-4} cm and 10^{-4} s; diffusion coefficients D_{ox}= D_{red}=10^{-5} cm^2/s; k_0=10^{-3} cm/s; the potential program started with positive scan direction from the actual redox potential (if c_{ox}=0 then from $E_0 - 0.3$ V) and changed linearly between the limits $E_0 - 0.3$ V and $E_0 + 0.3$ V for one or more complete cycles, with scan-rates typically between 10 mV/s and 0.2 V/s in 1-2-5 steps. Unless otherwise noted in the respective figure legend, the concentrations are c_{ox}=0 and c_{red}=10^{-6} mol/cm^3; the charge transfer coefficients are α_c=α_a=0.5; the uncompensated solution resistance is R_s=0.

The first simulation, Fig.3, is a somewhat extended version of Fig.2 of Ref. 2. It was the simplest case, with the parameters as listed above, i.e. only with one redox component present, and the first cycle has been simulated only.

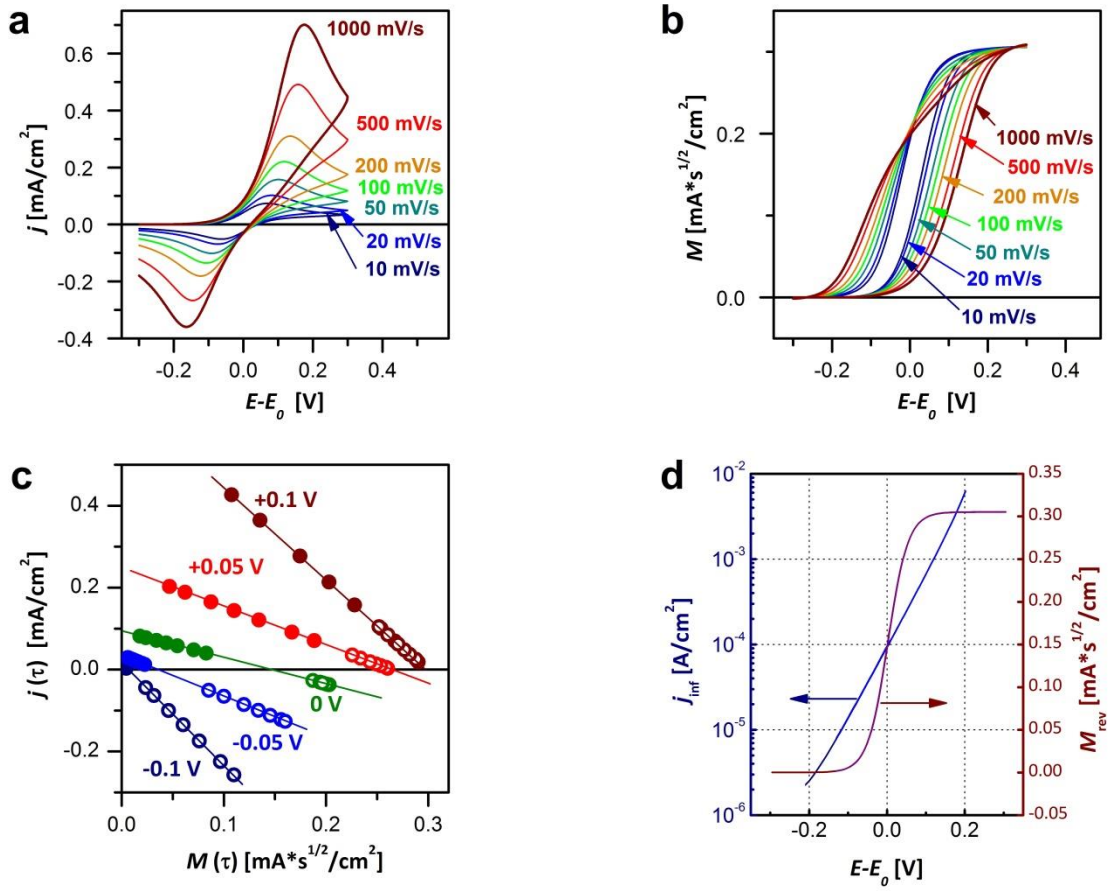

Figure 3. (a) Simulated CVs of scan-rates as indicated, c_{red}=10^{-6} mol/cm^3; for other parameters see the text. (b). The semiintegrated CVs. (c) The $j(\tau)$ vs $M(\tau)$ points for potentials as indicated. Full and open symbols are for anodic and cathodic scan directions, respectively. Outermost and innermost points on the lines are for the largest and smallest scan rates, respectively. (d) The $j_{\mathrm{inf}}(E)$ and $M_{\mathrm{rev}}(E)$ functions.

With the next simulation of Fig.4 we demonstrate that the $j_{\mathrm{inf}}(E)$ and $M_{rev}(E)$ functions do not change even after a number of cycles. Apart that the charge transfer coefficients have been changed to α_c=0.3 and α_a=0.7, ten cycles of the CV have been calculated. To avoid scrambled plots only the first and the tenth cycles of the CVs and the semiintegrated forms, and only for two scan-rates, are plotted. Note that the $j_{\mathrm{inf}}(E)$ and $M_{rev}(E)$ functions calculated from the first and tenth cycles are indistinguishably close to each other.

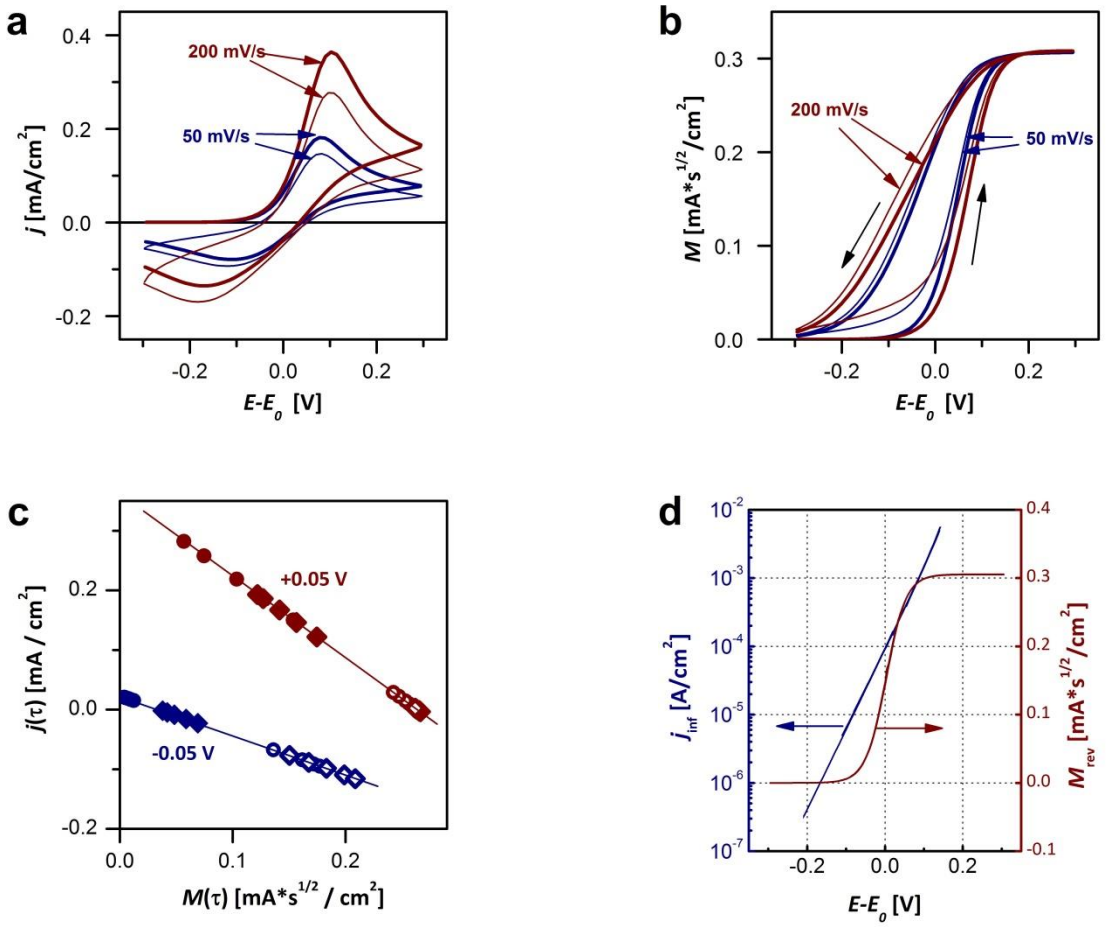

Figure 4. Simulated CVs and their transforms. For the meaning of (a) to (d) see the legend of Fig.3. Simulation parameters are the same as of Fig.3, but α_c=0.3 and α_a=0.7; and ten cycles have been calculated. Data of the first and the tenth cycles of CVs of 50 and 200 mV/s scan-rates are shown in Figs (a) and (b). The *j-M* linearity is demonstrated in (c) for two potentials as indicated. Circles and diamonds are data for the first and tenth cycles, respectively; full and open symbols are for anodic and cathodic scan directions, respectively. (d) The $j_{\mathrm{inf}}(E)$ and $M_{\mathrm{rev}}(E)$ functions.

With simulation of Fig.5, we demonstrate how we can get a "classical Tafel-plot". The parameters are the same as for the simulation of Fig.3, but both components of the redox system are present of equal concentrations (c_{ox}=c_{red}=5*10^{-7}). Note that the $\log(j)$ vs E curve is a typical Tafel plot of a 1:1 redox system; the M vs E curve exhibits one negative and one positive plateaus.

With the simulations of Fig.6 we demonstrate the elimination of the effect of IR drop. Note that the IR drop substantially distorts the CVs; still the transformed functions plotted on the IR-drop corrected potential scale are hysteresis-free functions.

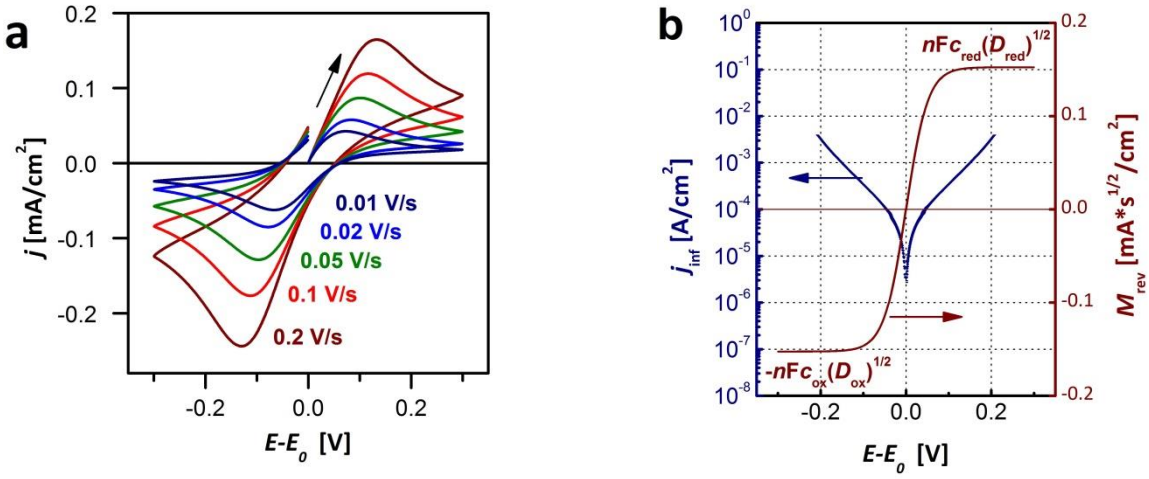

Figure 5. (a) Simulated CVs of scan-rates as indicated, c_{ox}=c_{red}=5*10^{-7} mol/cm^3; for other parameters see the text. (b) The $j_{inf}(E)$ and $M_{rev}(E)$ functions.

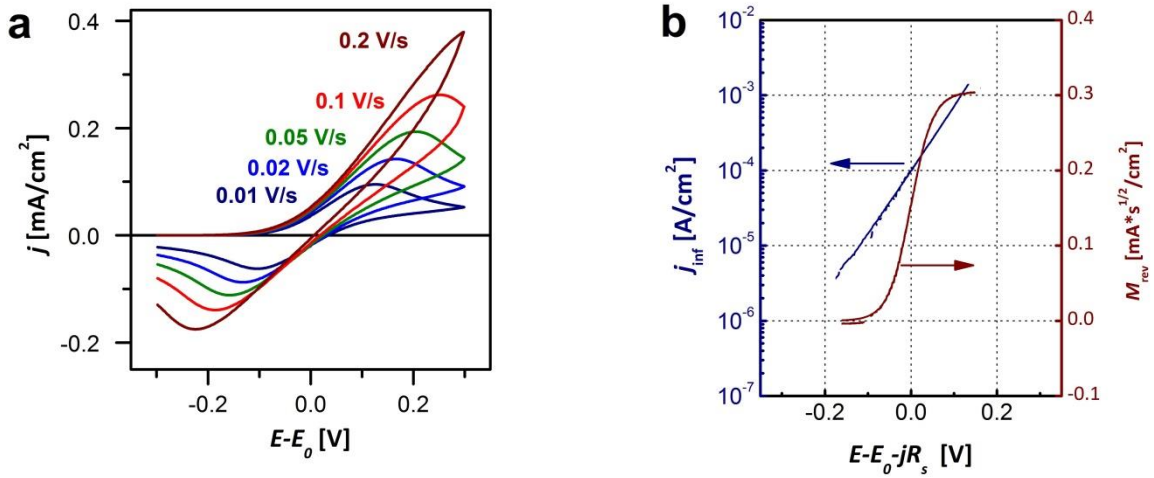

Figure 6. (a) Simulated CVs of scan-rates as indicated, c_{red}=10^{-6} mol/cm^3, R_s=200 Ohm*cm^2; for other parameters see the text. (b) The j_{inf} and M_{rev}: functions .against the IR-drop corrected potential.

The simulation of Fig.7 demonstrates that the transformation can be well applied also to voltammograms measured with time-varying scan-rates. Simulation parameters are the same as for Fig.3, but instead of five separate CVs, one continuous CV with a time-varying scan-rate (see the inset) has been simulated and transformed. The transformed $j_{\mathrm{inf}}(E)$ and $M_{rev}(E)$ functions are again the same hysteresis-free functions as of the previous simulations.

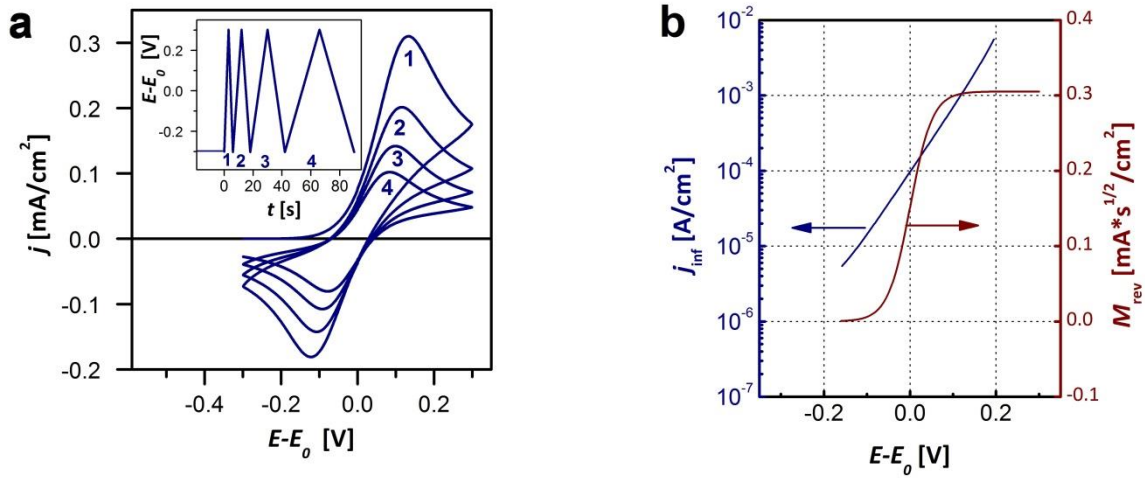

Figure 7. (a) Simulated CVs of scan-rates as indicated, c_{red}=10^{-6} mol/cm^3, for other parameters see the text. One continuous four-cycles CV with a time-varying scan-rate (see the inset on (a)) has been simulated and transformed. (b) The $j_{\mathrm{inf}}(E)$ and $M_{\mathrm{rev}}(E)$ functions.

3.2. Practical implication: determination of the charge transfer rate coefficients

3.2.1. Determination of H

In principle, this measurement and its evaluation is straightforward. One has to measure one or more $j(t)$ voltammograms with varied scan-rates. First the measured $j(t)$ functions are to be semiintegrated (cf. Eq.4). For this, the algorithm of Ref. 9 is recommended. It is a "fast" algorithm which requires in the order of magnitude of $N \cdot \ln(N)$ multiplications, in contrast to conventional convolution algorithms [1,11,22] with N^2 multiplications. Afterwards, plotting the $j(M)$ points of the same ε potential yields the $j_{\mathrm{inf}}(\varepsilon)$and $M_{\mathrm{rev}}(\varepsilon)$. Unless we wish to use it for some electroanalytical purposes, the latter function can be disregarded; $j_{\mathrm{inf}}(E)$ – as a "Tafel plot" is to be analyzed further. There is another way to obtain data on kinetics: As it follows from Eq. 8, the $H = k_{\mathrm{a}}/\sqrt{D_{\mathrm{red}}} + k_{\mathrm{c}}/\sqrt{D_{\mathrm{ox}}}$ parameter combination can be directly obtained by plotting $j_{\mathrm{inf}}/M_{\mathrm{rev}}$ as a function of potential. Note that an analogous coupling of *k* and *D* parameters appears when the

Faradaic impedance of the quasi-reversible redox system is theorized (cf. Eqs.3-11 [12]). The $j_{\text{inf}}/M_{\text{rev}}$ vs E plot for all simulated curves of Figs 3 to 5 are shown together in Fig.8.

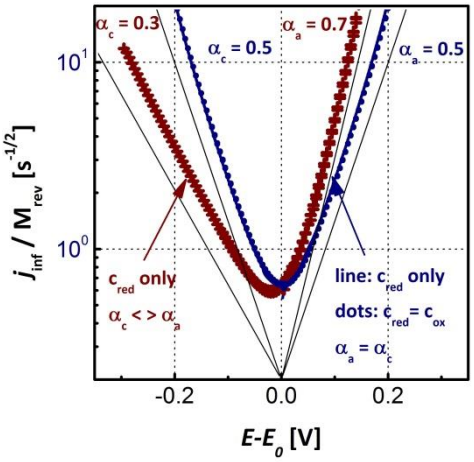

Figure 8. $j_{\text{inf}}/M_{\text{rev}}$ $\left[= H \equiv k_{\text{a}}/\sqrt{D_{\text{red}}} + k_{\text{c}}/\sqrt{D_{\text{ox}}}\right]$ vs E for the simulated data of Figs 3d, 4d and 5b (full circles, crosses and solid line, respectively). Additional thin lines represent the log(k) vs E slopes as calculated from the respective charge transfer coefficients. Note that $k_{\text{a}}/\sqrt{D_{\text{red}}} + k_{\text{c}}/\sqrt{D_{\text{ox}}}$ appears to be the same for the simulations with the reduced species only and with both components of the redox couple.

3.2.2. Complications

There might be complications mainly due to (i) the non-zero solution resistance (IR drop) and to (ii) double layer charging.

The IR drop effect is well known and it is easy to correct for [22]. Prior to – or following – the voltammetry measurements, one has to determine the solution resistance R_{s} by measuring an impedance spectrum at sufficiently high frequencies. Since all ε potentials of this text are of interfacial nature, the IR drop must be subtracted from the applied potential; i.e. we have to plot $j(M)$ points corresponding to the same $\varepsilon - jR_s$ potential, and analyse these plots to extract $j_{\text{inf}}(\varepsilon)$ and $M_{\text{rev}}(\varepsilon)$.

The charging current error is a more difficult issue, mostly because the double layer capacitance depends on electrolyte composition and electrode potential as well. One possible way of correction is based on “baseline-subtraction”: The voltammograms are to be measured with and without the redox component(s) added to the supporting electrolyte; then the difference of the voltammograms is to be analysed. Alternatively, “standard addition” might be also used: one

measures the voltammograms also with doubled concentration of the the redox component and then analyse the difference of the corresponding voltammograms.

3.2.3. Self-consistency

The $j_{\mathrm{inf}}(E)$ and $M_{rev}(E)$ plots provide a self-consistency check of the analysis. These plots should be, in principle, hysteresis-free; the $M_{rev}(E)$ function should exhibit the sigmoid shape of the "polarographic wave" expressed by Eq.15a; the potential dependence of $j_{\mathrm{inf}}(E)$ should be compatible with the Butler–Volmer equation. This feature, the demonstration of self-consistency is a big boon what we get when we apply the present theory for data analysis.

3.2.4. Alternatives

Compared to previously known techniques of voltammetric data analysis, the theory presented here opens a new route to determine rate and charge transfer (as well as diffusion) coefficients. Since the classical treatment of Nicholson [13] (see also Ch. 6.5.2 of [3]), kinetic parameters of the electrode reaction and diffusion coefficients are extracted from voltammetric signals based on theoretical relations of particular electrode reaction mechanisms, yielding k_0 values from CV peak separations.

Improved voltammetric analysis techniques described recently and used to determine kinetic parameters include, for example, statistical multivariable regression procedures applied to combined current–charge transients obtained from potentiostatic pulse experiments [14], multi-parameter estimation from hypersurface models [15,16], the use of artificial neural networks to distinguish voltammetric signals by reaction mechanism [17], bootstrap resampling to extract system parameters [18] and support vector or gaussian process regression based analyses [19]. As an alternative, fitting of simulated voltammetric features to experimental data may also be used for parameter extraction [20,21].

Both approaches — i.e., theoretical analyses and the fitting of simulated voltammograms — have their limitations, however. Theoretical relationships are only valid for certain kinetic schemes and mechanisms, while simulations, even if based on reasonable mechanistic hypotheses, usually take huge computation times and are extremely sensitive to parameter initialization [19].

As opposed to the afore-mentioned techniques, the method proposed here offers a relatively easy way of transforming voltammetric measurement results. The aim of this transformation is to decouple charge transfer and diffusion effects; the analysis of the $j(E)$ is left to a next step.

3.3. The novelty and general nature of the theory

The above theory is the generalized version of the one presented in Ref. [2] in three respects. (*i*) Both the oxidized and reduced components are assumed to be present rather than only one; (*ii*) For the derivation of Eq.9, no specific (e.g. exponential) dependence of the charge transfer rates on potential was needed; (*iii*) The theory applies to any arbitrary potential controlling waveform.

Apparently, Eq. 9 is a simple combination of five equations known and used for decades. In contrast to the previous semiintegration-based analysis methods [5,22,23,24], in which single CVs were analysed, we evaluate a set of voltammograms with different scan-rates together, or a single voltammogram comprising of multiple scans of arbitrarily changing scan-rates, or any combination of these. In the present way of analysis, there is an implicit scan-rate dependence involved; this is how we can extrapolate to ideally kinetics-controlled and transport controlled situations.

The scan-rate is a control parameter, *p*, which plays the role of tuning the ratio of rates of charge transfer and transport. There are other experimental techniques where some other time-related quantities play a similar role, as shown by Fig.9. In a special case of potential-jump experiments the linear $j(M)$ relation has been recognized by Oldham (cf. Eq. 11 of [11]): in these experiments, time can be considered a control parameter (Fig.9a). In impedance measurements (Fig.9b), where the Warburg term of the Faradaic impedance shrinks to yield the charge transfer resistance at the high frequency limit (see Ref. 3, Ch.10.4.1) it is the perturbation frequency that can be considered a control parameter. In case of rotating disk electrode experiments (Fig.9c) it is the rotation rate that plays the role of a control parameter (cf. to the Koutecký–Levich equation [25], see also Ref. 3, Ch.14.4.1).

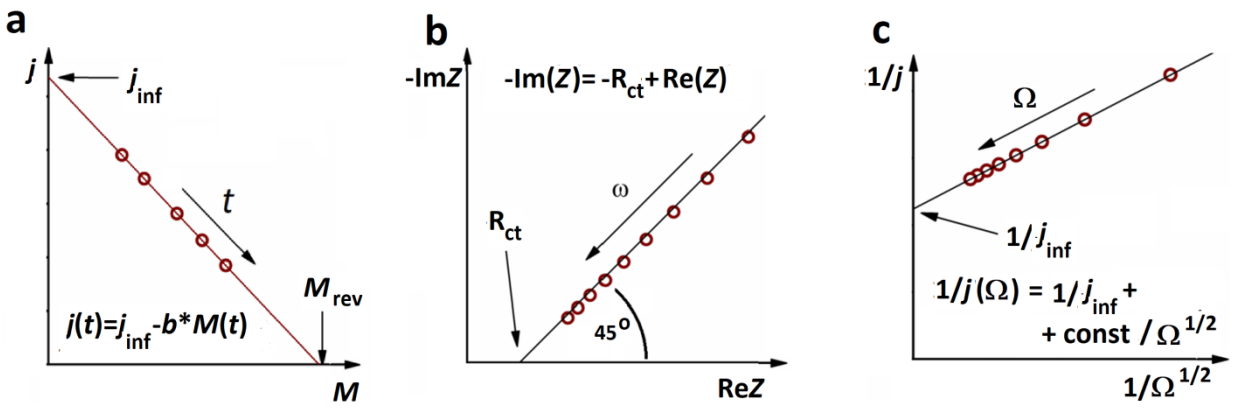

Figure 9. Analogue experiments for separation of the kinetics of diffusion and charge transfer by varying a control parameter *p.* For the present theory of (cyclic) voltammetry *p* is the scan-rate, *v*. (see also Fig.2). For other techniques:

a. For chronoamperometric transients *p* is time, *t* (cf. Oldham's procedure, Eq. 11 of [11])

b. In impedance spectroscopy *p* is frequency, ω (Faraday impedance = R_{ct}-W)

c. For a rotating disc electrode *p* is rotation speed, Ω (cf. the Koutecky-Levich equation)

4. Conclusions

The theory presented here, along with the illustrating simulations, shows how to transform quasi-reversible voltammograms to yield two scan-rate independent functions. One of them is characteristic to charge transfer kinetics, the other to diffusional flux. From an algebra point of view, Eq. 9 is a simple combination of five well-known equations pertinent to the voltammetry of quasi-reversible redox systems. In Eq. 9 we make use of the implicit scan-rate dependence of the current and of its semiintegral at a constant potential. In other words, the two functions are determined from a set of voltammograms of different scan-rates or from voltammograms comprising a number of cycles with varied scan-rates.

The theory leading to Eq.9 opens a new route for the determination of charge transfer rate coefficients of quasi-reversible redox systems.

Acknowledgements:

The research within project No. VEKOP-2.3.2-16-2017-00013 was supported by the European Union and the State of Hungary, co-financed by the European Regional Development Fund. Additional support of the Hungarian Science Research Fund OTKA (No. K112034) is acknowledged. S. Vesztergom acknowledges the support of the National Research, Development and Innovation Office of Hungary under the grant NKFIH PD–124079.

List of symbols

E, t	electrode potential and time, in general
ε, τ	ε is the electrode potential at time τ
$E_{0,} E_{1/2}$	standard redox potential and half-wave potential
v	scan rate
j	current density
j_{inf}	current density at infinite transport rate
M	semiintegrated current density (cf. Eq.3)
M_{rev}	semiintegrated current density for reversible redox systems
$M_{\text{lim,a}}, M_{\text{lim,c}}$	anodic and cathodic limit values of M_{rev}
$c_{\text{red}}, c_{\text{ox}}$	concentration of the reduced and oxidized species in the electrolyte bulk
$c_{\text{red}}^{\text{s}}, c_{\text{ox}}^{\text{s}}$	concentration of the reduced and oxidized species at the electrode surface
$D_{\text{red}}, D_{\text{ox}}$	diffusion coefficient of the reduced and oxidized species
k_{a} , k_{c} , k_0	rate coefficient of the anodic and cathodic reactions, and standard rate coefficient
α_{a} , α_{c}	charge transfer coefficient of the anodic and cathodic reactions
H,K	parameter combination of k_{a} , k_{c} , D_{red}, and D_{ox} (cf. Eqs.6 and 10).
n	charge number of the electrode reaction
F,R,T	Faraday's number, universal gas constant, temperature

References:

1 K.B. Oldham, A signal-independent electroanalytical method, *Anal. Chem*, **44** (1972) 196.

2 T. Pajkossy, Analysis of quasi-reversible cyclic voltammograms: Transformation to scanrate independent form, *Electrochem. Comm.* **90** (2018) 69.

3 A.J. Bard, L.R. Faulkner, Electrochemical Methods, 2nd ed. Wiley, 2001, ISBN: 978-0-471-04372-0

4 H.Matsuda, Y.Ayabe, To the theory of the Randles-Sevčik cathode-ray polarography (in German), *Z. Elektrochemie* **59** (1955) 494.

5 K.B. Oldham, J.C. Myland, A.M. Bond, Electrochemical science and technology: fundamentals and applications, Wiley, 2012, ISBN 978-0-470-71085-2, Ch.12.

6 R. Guidelli, R.G. Compton, J.M. Feliu, E. Gileadi, J. Lipkowski, W. Schmickler, and S.Trasatti, Definition of the transfer coefficient in electrochemistry (IUPAC Recommendations 2014), *Pure Appl. Chem.* **86** (2014) 259

7 K.B. Oldham, G.D. Zoski, Effect of semioperators on reversible cyclic voltammograms, *Anal. Chem*. **52** (1980), 2116.

8 S. Vesztergom, A short introduction to digital simulations in electrochemistry: Simulating the Cottrell experiment in NI LabVIEW, *J. Electrochem. Sci. Eng.* **8** (2018) 171.

9 T. Pajkossy, L. Nyikos, Fast algorithm for differintegration, *J. Electroanal. Chem*. **179** (1984) 65.

10 P.R. Bevington, D.K. Robinson, Data reduction and error analysis for the physical sciences, 3d ed. McGraw-Hill, 2003, ISBN-10: 0072472278, Ch.6.

11 K.B. Oldham, The extraction of kinetic parameters from chronoamperometric or chronocoulometric data, *J. Electroanal. Chem*., **145** (1983) 9.

12 R. de Levie, L. Pospisil, On the coupling of interfacial and diffusional impedances, and on the equivalent circuit of an electrochemical cell, *J. Electroanal. Chem*. 22 (1969) 277.

13 R.S. Nicholson, Theory and application of cyclic voltammetry for measurement of electrode reaction kinetics, *Anal. Chem*. **37** (1965) 1351.

14 C. Barbero, M. A. Zón, H. Fernández, The extraction of heterogeneous kinetic parameters from combined cbronoamperometric and chronocoulometric data by a multiple regression procedure, *J. Electroanal. Chem*. **265** (1989) 23.

15 B. Scharbert, B. Speiser, Chemical information from electroanalytical data. Part 1 — Determination of system parameters for quasi-reversible electron transfer reactions from cyclic voltammetric test data and data for the reduction of cerium(IV) bis(octaethylporphyrinate). *J. Chemometrics* **3** (1989) 61.

16 B. Speiser, Chemical information from electroanalytical data. Part 2. Determination of the rate and equilibrium constants of a chemical reaction preceding a reversible electron transfer from cyclic voltammetric data, *J. Electroanal. Chem*. **301** (1991) 15.

17 E. P. Sapozhnikova, M. Bogdan, B. Speiser, W. Rosenstiel, EChem++ — An object-oriented problem solving environment for electrochemistry. Part 3. Classification of voltammetric signals by the fuzzy ARTMAP neural network with respect to reaction mechanism, *J.Electroanal. Chem.* **588** (2006) 15.

18 L. K. Bieniasz, H. Rabitz, Extraction of parameters and their error distributions from cyclic voltammograms using bootstrap resampling enhanced by solution maps: Computational study, *Anal. Chem*. **78** (2006) 8430.

19 M. Bogdan, D. Brugger, W. Rosenstiel, B. Speiser, Estimation of diffusion coefficients from voltammetric signals by support vector and gaussian process regression, *J. Cheminformatics* **6** (2014) 30.

20 M. Rudolph, D. P. Reddy, S. W. Feldberg, A simulator for cyclic voltammetric responses, *Anal. Chem*. **66** (1994) 589A.

21 A. W. Bott, S. W. Feldberg, M. Rudolph, Fitting experimental cyclic voltammetry data with theoretical simulations using Digisim 2.1., *Curr. Sep.* **15** (1996) 67.

22 J.C. Imbeaux, J.M. Savéant, Convolutive potential sweep voltammetry, I. Introduction, *J. Electroanal. Chem*. **44** (1973) 169.

23 K.B. Oldham, J.C. Myland, Extracting parameter values from quasireversible cyclic voltammograms, *J Solid State Electrochem*. **16** (2012) 3691.

24 A.Neudeck, F.Marken, R.G. Compton, Complex electron transfer kinetic data from convolution analysis of cyclic voltammograms. Theory and application to diamond electrodes, *Electroanalysis* **11** (1999) 1149.

25 J. Koutecky, V.G. Levich, Application of a rotating disk electrode to the study of kinetic and catalytic processes in electrochemistry (in Russian), *Zh. fiz. khim*. **32** (1958) 1565.